

## Dynamics and Topology of Symmetry Breaking with Skyrmions

J. Pišljarić<sup>1</sup>, A. Nych<sup>1,2</sup>, U. Ognysta<sup>2</sup>, A. Petelin<sup>3,5</sup>, S. Kralj<sup>1,4</sup> and I. Muševič<sup>1,5</sup>

<sup>1</sup>Condensed Matter Department, J. Stefan Institute, Jamova cesta 39, 1000 Ljubljana, Slovenia

<sup>2</sup>Department of Molecular Photoelectronics, Institute of Physics, Nauky Prospect 46, Kyiv 03680, Ukraine

<sup>3</sup>Complex Matter Department, J. Stefan Institute, Jamova cesta 39, 1000 Ljubljana, Slovenia

<sup>4</sup>Department of Physics, Faculty of Natural Sciences and Mathematics, University of Maribor, Koroška cesta 160, 2000 Maribor, Slovenia

<sup>5</sup>Faculty of Mathematics and Physics, University of Ljubljana, Jadranska 19, 1000 Ljubljana, Slovenia

 (Received 18 May 2023; revised 11 December 2023; accepted 11 January 2024; published 22 April 2024)

We observe that pretransitional order parameter fluctuations of a skyrmion-forming chiral nematic liquid crystal are slowed down for 4 orders of magnitude, if confined to  $\lesssim 100$  nm thin layers. Fluctuating fragments of half-skyrmions are observed in a narrow temperature interval and are explained by thermally activated hopping between the various energy states. Skyrmion fluctuations are accompanied by imbalanced topological charge: positive charges appear at higher temperatures and dominate in the fluctuating region until skyrmions fully condense and negative charges appear at lower temperatures.

DOI: [10.1103/PhysRevLett.132.178101](https://doi.org/10.1103/PhysRevLett.132.178101)

Skyrmions are topologically protected structures of a particular field that cannot be smoothly removed or unwound into a homogeneous field. They were first proposed by Skyrme to describe particlelike excitations of the pion field [1]. Since then, skyrmions have been observed as magnetic vortices in chiral magnets [2,3], in spinor Bose-Einstein condensates [4], and chiral nematic liquid crystals (LCs) [5–10]. Here, they spontaneously emerge by cooling from the isotropic phase (I) into one of the 3D skyrmion phases, such as the Blue Phases (BPs) I, II, and III [11]. The phase transition into the BPs not only results in spontaneous formation of order through symmetry breaking, but gives birth to topologically protected skyrmions. This double nature of the isotropic-BP transition therefore opens a question regarding how these topologically protected and complex 3D structures can spontaneously form.

In this Letter we report on direct observation and imaging of half-skyrmion (HS) condensation near the I-HS phase transition in  $\sim 80$  nm thin BPI layers. The I-BPI transition is first order in bulk, but becomes gradual, when the material is confined to layers below the critical thickness  $d_c$  of capillary condensation [12–15]. We observe thermally excited formation and disappearance of individual HSs, when the thickness of BPI layer is lower than  $d_f > d_c$ ,  $d_f \sim 70$  nm. The lifetime of skyrmions and their parts increases, as the temperature is lowered, until skyrmions fully condense into a liquid of HS. Chiral fluctuations in this region are slowed, compared to bulk [16], for more than 4 orders of magnitude by the effect of confinement, which enables us to image and measure the skyrmion fluctuations that were to our knowledge never observed before.

The experiments were performed in thin layers of chiral LC mixtures with a pitch of 360 nm and 710 nm [10,17]. To provide (weak) planar-degenerate anchoring conditions [18], bare and polymethyl methacrylate covered glass slides were used to producing wedgelike LC layers, with thickness from  $\sim 30$  nm to a few 100 nm [11]. The LC was observed using a diffraction limited optical microscope in reflection mode with NA = 1.45 oil-immersion objective and narrow spectral band of illumination light centered around  $\lambda = 450$  nm yielding optical resolution of  $\sim 150$  nm. The temperature of the LC was controlled to  $\sim 4$  mK.

Figure 1(a) shows a sequence of images of 360 nm-pitch LC at temperatures near the I-BPI transition and varying thickness between 60–90 nm (Supplementary Video (SV) 1). In thicker parts ( $\sim 90$  nm) we observe a typical first-order transition, where the HS phase grows in form of plateletlike clusters, shown in Fig. 1(b). A single HS or a cluster of a few HSs appears instantaneously from the I phase and acts as nucleation site for further growth. The doughnutlike appearance of HSs with a dark center is a consequence of refractive index mismatch between the glass and the local molecular orientation [inset to Fig. 1(a)] [10,11,34].

Just below the thickness  $d_f$  (dashed vertical line), we observe pronounced visual flickering of round bright domains of  $\sim 100$ – $300$  nm size. It is on the timescale of  $\sim 10$ – $100$  ms, and is clearly visible to the bare eye. With decreasing thickness and lowering the temperature, the dynamically formed domains become elongated, spontaneously changing shape and closing into HS loops. They either decay back into a moonlike form or remain as individual HS within the I phase. The dashed squares 2

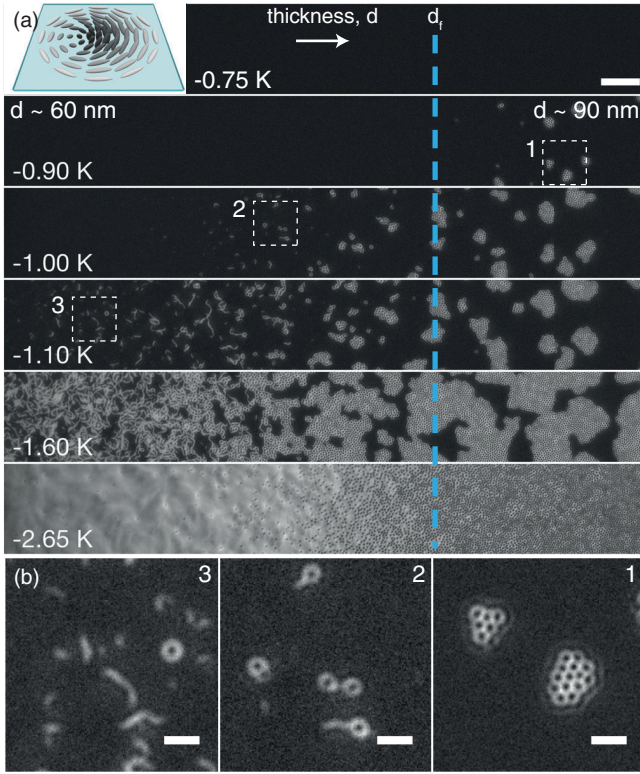


FIG. 1. (a) Each panel shows the same region of BPI LC in a wedge cell at different temperatures compared to the I-BPI transition in bulk. The thickness ranges from 60 nm (left) to 90 nm (right). The dashed vertical line denotes  $d_f$ , where fluctuations are first observed at the transition. The top inset shows the structure of a HS. Scale bar 5  $\mu\text{m}$ , images are taken with right-handed circularly polarized light and rescaled for contrast. Sequence is shown in SV 1. (b) Subfigures 1-3 depict enlargements of regions in (a) at the thickness of (1)  $\sim 80\text{--}82$  nm, (2)  $\sim 72\text{--}74$  nm, and (3)  $\sim 62\text{--}64$  nm. Scale bar 1  $\mu\text{m}$ .

and 3 in Fig. 1(a) denote regions with different thicknesses, with their details revealed in Fig. 1(b). For the thinnest regions in Fig. 1, the fluctuations are moonlike, but rarely form a doughnut. This means that the formation of HS becomes energetically less favorable with decreasing thickness. Indeed, below  $d \sim 70$  nm the aerial density of HS drops rapidly [Fig. 1(a)], reminiscent of a dense HS liquid to gaseous HS phase transition.

Figure 2(a) shows a 1 s long sequence of a single region within the fluctuating regime. Differently colored circles denote different dynamic structures and types of fluctuations, which either form a HS (yellow) or appear and disappear as moonlike patches in the isotropic background (red). The dynamics in one region thus consists of several dynamic processes, which unfold at different rates. We used differential dynamic microscopy to measure dynamics of HS fluctuations [18,19,35]. Examples of obtained time-autocorrelation functions are shown in Fig. 2(b) for a few selected temperatures and image wave vector  $\bar{q} = 6.7 \mu\text{m}^{-1}$ . Typical frames at these temperatures are on the right of

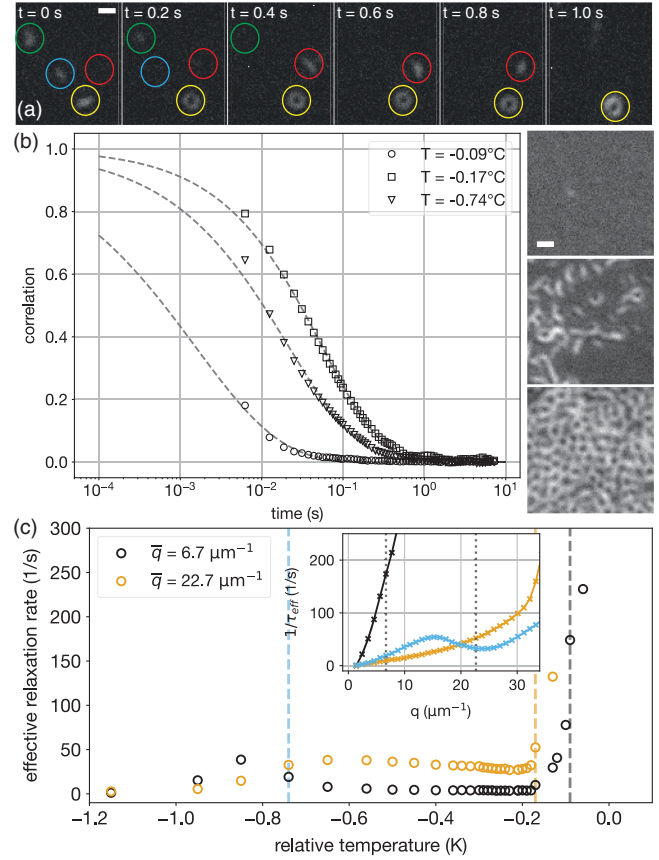


FIG. 2. (a) Different types of events occurring in a single second within the fluctuating region of a highly chiral LC. Scale bar 500 nm. (b) Autocorrelation functions (left) for three different temperatures at  $\bar{q} = 6.7 \mu\text{m}^{-1}$ , showing critical slowing down of skyrmion fluctuations due to symmetry breaking when cooling from the I phase. The images on the right were rescaled for contrast. Scale bar 500 nm. (c) Temperature dependence of effective relaxation rates ( $1/\tau_{\text{eff}}$ ) at two different image wave vectors:  $\bar{q} = 6.7 \mu\text{m}^{-1}$  (long wavelength limit) and  $\bar{q} = 22.7 \mu\text{m}^{-1}$  (comparable to HS size). The inset shows relaxation rate dispersion at three temperatures in (b), also marked with vertical dashed lines in (c).

Fig. 2(b) (see also SV 2). The functions were fitted to stretch-exponential function  $f(t) = ae^{-(t/\tau_{\text{eff}})^s}$ , which takes into account different relaxation events in the entire field of view [18] and the temperature dependencies of the fluctuations' relaxation rates  $1/\tau_{\text{eff}}$  are shown in Fig. 2(c). The inset of Fig. 2(c) shows the  $1/\tau_{\text{eff}}$  dependence on the image wave vector  $\bar{q}$  for the three temperatures indicated in Fig. 2(b).

The observed  $\sim 10^1\text{--}10^2$  Hz fluctuation rates [Fig. 2(c)] are 4 orders of magnitude slower compared to the  $\sim 10^6$  Hz nematic order parameter (OP) fluctuation rates at the I-BP transition [16]. This indicates a critical region with extremely flat OP thermodynamic potential, as discussed by H. Yokoyama [13], or a thermally activated hopping mechanism between local energy minima. The Landau de

Genes free energy of a chiral nematic is a sum of volume and surface contributions:  $F = \int (f_c + f_e) d^3\mathbf{r} + \int f_s d^2\mathbf{r}$ , where  $f_c$  and  $f_e$  are the condensation and elastic volume terms, and  $f_s$  is the surface free energy density, respectively [36]. When the LC is confined between two walls separated by  $d$  that enforce identical surface ordering, the spatially averaged dimensionless free energy density  $g(s)$  becomes [20]

$$g(s) = r(d, T)s^2 - 2s^3 + s^4 - \sigma s. \quad (1)$$

$s$  is the dimensionless amplitude of the OP and we consider single elastic constant and uniaxial approximation, with homogeneous  $s$ —see Ref. [18] for an extended derivation. In Eq. (1),  $r(d, T) = (T - T^*)/(T_{\text{IN}} - T^*) + (\xi_{\text{IN}}^2/d^2)g_e + (2\xi_{\text{IN}}^2)/(d \cdot d_e^{(2)})$  is the effective dimensionless temperature that drives the transition into the ordered phase,  $\xi_{\text{IN}}$  is phase transition correlation length,  $d_e^{(i)}$  are the ordering ( $i = 1$ ) and disordering ( $i = 2$ ) surface extrapolation lengths [36], and  $\sigma = (\xi_{\text{IN}}^2/d^2)g_{24} + (2\xi_{\text{IN}}^2)/(d \cdot d_e^{(1)})$  is the dimensionless effective ordering field. Dimensionless parameters  $g_e$  and  $g_{24}$  quantify elastic distortions in the director field:  $g_e = (1/2d) \int [(\nabla \cdot \mathbf{n})^2 + (\mathbf{n} \cdot (\nabla \times \mathbf{n}) - q)^2 + |\nabla \times \mathbf{n}|^2] d^3\mathbf{r}$  is the energy penalty for deformation deviating from simple splay, twist, and bend in confinement, and  $g_{24} = (1/d) \int \nabla \cdot (\mathbf{n} \nabla \cdot \mathbf{n} - (\nabla \mathbf{n}) \mathbf{n}) d^3\mathbf{r}$  is the energy penalty for saddle-splay deformation. The shift  $\Delta T(d)$  of the order-disorder phase transition (coexistence) temperature in confinement is [18]

$$\Delta T(d) = (T_{\text{IN}} - T^*) \left[ \frac{\xi_{\text{IN}}^2}{d^2} (g_{24} - g_e) + \frac{2\xi_{\text{IN}}^2}{d} \left( \frac{1}{d_e^{(1)}} - \frac{1}{d_e^{(2)}} \right) \right]. \quad (2)$$

If the surface prefers ordered nematic ( $d_e^{(1)} < d_e^{(2)}$ ),  $\Delta T(d)$  is positive, and is negative for surfaces preferring disorder [13,20]. The generic  $(T, d)$  phase diagram in the inset of Fig. 3(a) shows a first-order phase boundary that ends in a critical point  $CP$  (marked with a red point), determined by  $\sigma = \sigma_c = 0.5$ , below which the transition is gradual—see also Fig. 4(b) in [18]. The experimentally determined  $(d, T)$  phase diagram is shown in main Fig. 3(a), with the black curve of the form  $T(d) = T_0 - A/d$ . The blue color gradient marks a region in which the transition from the high-temperature phase becomes gradual with reducing thickness, including the fluctuating region. It is not possible to say in this case the transition disappears at a sharply defined critical thickness, but rather the transition into the critical region is gradual itself, with the critical thickness  $d_c \lesssim 50$  nm. Figure 3(b) shows the three different transition regimes: in thick regions (right), stable HS clusters nucleate in bulk or at the surfaces that grow quickly once the transition temperature is reached [see Fig. 1(b) (1)].

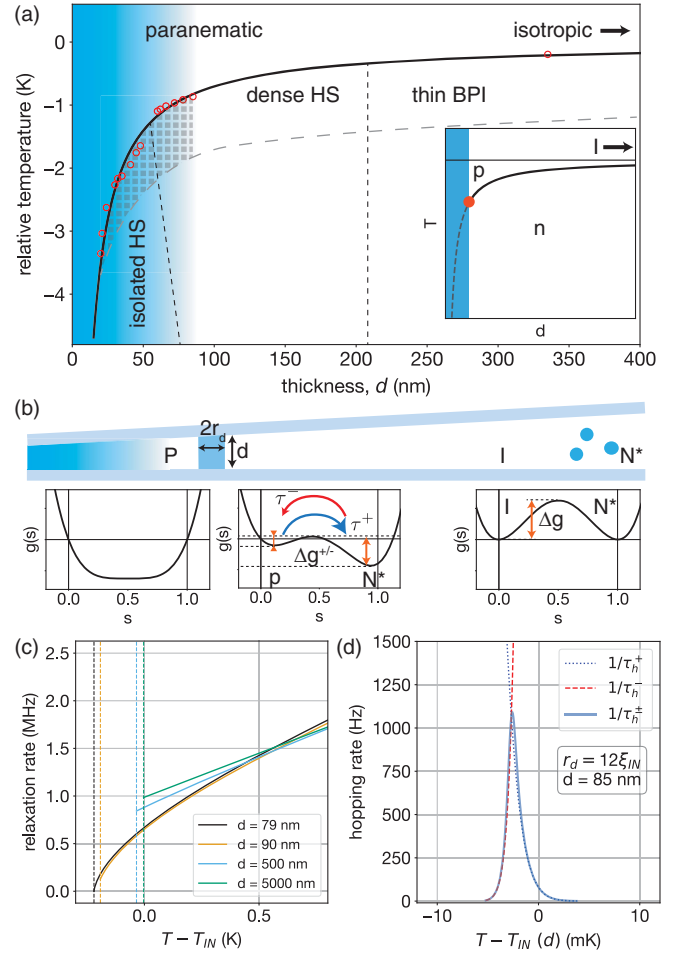


FIG. 3. (a)  $(T, d)$  phase diagram. The blue gradient represents a gradual change of phase transition nature with thickness and the fluctuations are observed roughly in the square-patterned region. The inset shows theoretically predicted phase diagram with critical point (red dot). (b) Schematic of three phase transition types observed in confined LCs (above) and schematic free energy  $g(s)$  OP dependencies of different thicknesses. (c) Temperature dependence of OP relaxation rate in the I phase at different thicknesses. (d) Temperature dependencies of the hopping rate between the two equilibrium states at  $d = 85$  nm ( $d_c = 79$  nm in this model).

Local minima at  $s = s_n \sim 1.0$  and  $s = s_p \sim 0$  here represent the ordered (nematic) and disordered phase (confined isotropic—paranematic), respectively. In the fluctuating region (central schematic), the condensation energy barrier  $\Delta g_{\text{cond}}^{+/-}$  is strongly reduced due to confinement, while the barrier disappears completely at lower  $d \lesssim d_c$  (shown left)—this point is discussed in more detail below.

We calculated the relaxation rates  $\tau^{-1}$  of the OP fluctuations around the equilibrium, given by the local curvature of  $g(s)$  minima,  $\tau^{-1} = \tau_{\text{IN}}^{-1} \cdot g_i^{(2)}$ , where  $g_i^{(2)} = \partial^2 g / \partial s^2|_{s=s_i}$ ,  $i = n, p$ . Next,  $\tau_{\text{IN}}^{-1}$  is the OP relaxation rate in bulk, which is of the order of  $10^6$  Hz for a typical I-N/BP transition. The calculated temperature dependence of the

OP relaxation rates  $\tau^{-1}$  are shown in Fig. 3(c) for various  $d$ —see Table 1 in [18] for values of numerical parameters used. The relaxation rates drop down to  $\sim 10$  Hz only in a very narrow ( $\sim 1$   $\mu$ K) interval and around the critical thickness ( $d_c = 79$  nm) for selected set of parameters. This is 4 orders of magnitude narrower than observed in the experiments and in apparent discrepancy to the simple Landau theory and the soft mode approach for the bulk phase transition [37].

The clue to this puzzle is hidden in the size of the fluctuating HS fragments, which is around  $\sim 200$  nm, as seen from Fig. 1(b). For a local thickness of  $\sim 60$ – $80$  nm, the fluctuating HS fragments are actually chiral capillary bridges stochastically forming between the two surfaces. Capillary condensation in very thin nematic layers has been observed by Kočevár *et al.* [15,38,39].

We consider a cylindrical capillary bridge of radius  $r$  and height  $d$  [Fig. 3(b)] as the state in a local minima at  $s_n$  and the absence of the capillary bridge corresponding to local minimum with  $s_p < s_n$ . The maximum between the minima appears at  $s_m$ . The times for hopping between the two free-energy minima, separated by a barrier of height  $\Delta G^\pm$ , are  $\tau_h^\pm = \tau \cdot e^{\beta \Delta G^\pm}$ , where  $\beta = 1/k_B T$  and  $\tau$  is the relaxation time in the currently occupied minimum.  $\Delta G^\pm$ , and consequently  $\tau_h^\pm$ , are different for  $N \rightarrow I$  (–) and  $I \rightarrow N$  (+) jumps.  $\Delta G^\pm$  is composed of two parts: (i) the free energy needed to condense an ordered capillary bridge (and vice versa),  $G_{\text{cond}}^\pm$  and (ii) the energy cost of the formation of the interface between the nematic bridge and surrounding paranematic phase  $G_{\text{intrf}}$  (and vice versa). The free energy related to condensation of the nematic bridge is  $G_{\text{cond}} = a_0(T_{\text{IN}} - T^*)S_0^2 \Delta g^\pm \pi r^2 d$ , with  $\Delta g^{+/-} = g(s_m) - g(s_{p/n})$  and the corresponding energy for the creation of (chiral)  $N$ -paranematic interface is  $G_{\text{intrf}} = \gamma_{\text{IN}}^0 (s_n - s_p)^2 2\pi r d \sqrt{g_n^{(2)}}$  [18,21,40]. Here,  $a_0$  is the leading coefficient of the Landau expansion,  $T_{\text{IN}}$  the bulk transition temperature,  $S_0$  the value of OP at the transition in bulk, and  $g(s_i)$ ,  $i = n, p$ , are the free-energy densities in the nematic and paranematic phases.  $\gamma_{\text{IN}}^0$  is bare I-N interfacial tension. The hopping times  $\tau_h^\pm$  are

$$\frac{\tau_h^\pm}{\tau_{\text{IN}}} = \frac{\exp[\beta(G_{\text{cond}}^\pm \pm G_{\text{intrf}}^\pm)]}{g_i^{(2)}}. \quad (3)$$

Figure 3(d) shows the temperature dependence of the two hopping rates  $1/\tau_h^\pm$ , calculated for  $d = 85$  nm and  $r = 12\xi_{\text{IN}}$ , which are now 1000 times slower compared to OP fluctuations, shown in Fig. 3(c), and comparable to experiments. Also, the temperature interval of high hopping rates is now of the order of few mK for this set of parameters [18]. This temperature range depends strongly on the surface anchoring strength, and even small local variation of the surface anchoring strength [41,42] of  $\sim 5\%$ ,

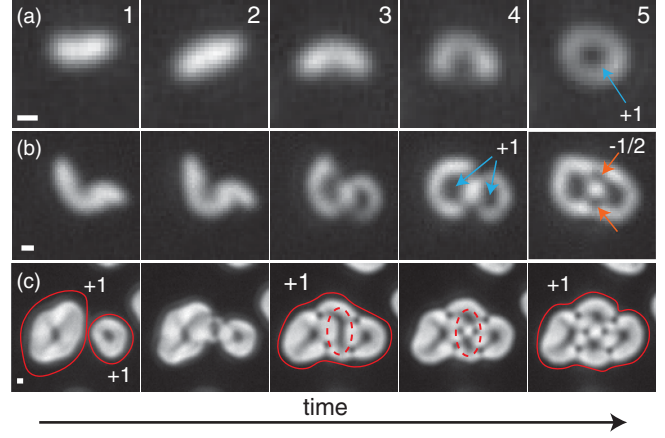


FIG. 4. Formation of (a) a single and (b) two HSs from the I phase. Note the circular shape of the HS in image 5 of (a), indicating the absence of two  $-1/2$  disclination lines, representing excess of positive charge of  $+1$  per HS. Note the appearance of the two  $-1/2$  disclination lines when two connected HSs are formed in image 5 of (b), keeping the total topological charge of a merged cluster to  $+1$ . (c) Merging of HS upon cooling, which partially compensates the total topological charge of all the HSs. Because of  $-1/2$  disclinations, the total winding of an island remains  $+1$  (encircled red), regardless of merging with other HSs. Additional HSs within the islands (dashed red ellipse) can form by splitting a HS into two, with simultaneous appearance of  $-1/2$  disclinations. All images were taken in the longer pitch LC. Scale bars in (a)–(c) represent 200 nm. All sequences are from SV 3.

results in shifting the local temperature of phase transition for  $\sim 40$  mK, thereby broadening the temperature window of vivid skyrmion fluctuations.

The paranematic-skyrmion phase transition not only breaks the continuous symmetry of the disordered phase, but also changes the topology of the orientational field considered topologically charge-neutral at all times. Figure 4(a) shows a formation of a single HS in a longer pitch material at thickness of  $d \sim 120$  nm, following a temperature quench: elongated domains form (1–2), develop a kink (3) and bend (4) inward until a HS is formed (5). Considering the paranematic surrounding, each new HS carries a topological charge  $+1$  and there is an excess of positive charge, because the  $-1/2$  disclination lines are not observed at this stage. Further, Fig. 4(b) presents a formation of a pair of HSs, starting as a wavy, moonlike feature (1–2) that closes into a pair of tightly bound HSs (3–4) on both sides. Two dark indentations (3–4) on the surface of the connecting neck are the seeds of two  $-1/2$  disclination lines that become clearly visible (5). The  $-1/2$  charge disclination lines are generated only via collision and merging of individual HSs, reducing the positive charge of a cluster to  $+1$ . This imbalance is also observed in other events, as shown in Fig. 4(c). Once two or more HS clusters collide (1), strong bending of the director at the touching surfaces occurs (2), which is relieved through the formation of  $-1/2$  disclinations (3–5),

balancing the total winding number to  $+1$ . In the fluctuating regime observed in a shorter pitch material, such events are reversibly driven by thermal energy, changing the total charge on a millisecond timescale. The excess positive charge is neutralized at lower temperatures via HS merging that generates negative charge. This behavior does not violate the conservation of topological charge, but simply classifies topological charges into two classes: (i) the “real charge” is observable as a singularity in the centers of individual HSs and (ii) the “evanescent charges” remain undetected in the paranematic phase, as the amplitude of the order is below the detection limit of the instrumentation used. For details see Ref. [18].

We note that the fluctuations of skyrmions shown in Figs. 1, 2, and 4 can be viewed as fluctuations and slowing down of double-twist eigenmode, considered by Long and Selinger [43] as the lowest energy mode in chiral nematic LCs in cylinders with free boundary conditions.

In conclusion, the results reveal an extremely slowed-down dynamics of topologically nontrivial double-twisted structures—skyrmions in confinement, and surprising imbalance of skyrmion topological charge in a narrow temperature interval exhibiting strong fluctuations. This may be of fundamental importance for topological phase transitions in general and for symmetry-breaking dynamics in nonequilibrium first-order phase transitions in particular [44].

This work was supported by Slovenian Research Agency (ARRS) through Contracts No. P1-0099 (I. M.), No. PR-08332 (J. P.). A. N. and U. O. acknowledge support from NAS Ukraine (Grant No. 1.4.B/209).

---

[1] T. H. R. Skyrme, A unified field theory of mesons and baryons, *Nucl. Phys.* **31**, 556 (1962).  
 [2] U. K. RöSSLer, A. N. Bogdanov, and C. Pfeleiderer, Spontaneous skyrmion ground states in magnetic metals, *Nature (London)* **442**, 797 (2006).  
 [3] S. Mühlbauer, B. Binz, F. Jonietz, C. Pfeleiderer, A. Rosch, A. Neubauer, R. Georgii, and P. Boni, Skyrmion lattice in a chiral magnet, *Science* **323**, 915 (2009).  
 [4] A. E. Leanhardt, Y. Shin, D. Kielpinski, D. E. Pritchard, and W. Ketterle, Coreless vortex formation in a spinor Bose-Einstein condensate, *Phys. Rev. Lett.* **90**, 140403 (2003).  
 [5] M. Kawachi, O. Kogure, and Y. Kato, Bubble domain texture of a liquid crystal, *Jpn. J. Appl. Phys.* **13**, 1457 (1974).  
 [6] W. E. L. Haas and J. E. Adams, Electrically variable defraction in spherulitic liquid crystals, *Appl. Phys. Lett.* **25**, 263 (1974).  
 [7] N. Nawa and K. Nakamura, Observation of forming process of bubble domain texture in liquid crystals, *Jpn. J. Appl. Phys.* **17**, 219 (1978).  
 [8] A. N. Bogdanov, U. K. RöSSLer, and A. A. Shestakov, Skyrmions in nematic liquid crystals, *Phys. Rev. E* **67**, 016602 (2003).

[9] I. I. Smalyukh, Y. Lansac, N. A. Clark, and R. P. Trivedi, Three-dimensional structure and multistable optical switching of triple-twisted particle-like excitations in anisotropic fluids, *Nat. Mater.* **9**, 139 (2009).  
 [10] A. Nych, J. Fukuda, U. Ognysta, S. Žumer, and I. Mušević, Spontaneous formation and dynamics of half-skyrmions in a chiral liquid-crystal film, *Nat. Phys.* **13**, 1215 (2017).  
 [11] J. Pišljari, S. Ghosh, S. Turlapati, N. Rao, M. Škarabot, A. Mertelj, A. Petelin, A. Nych, M. Marinčič, A. Pusovnik, M. Ravnik, and I. Mušević, Blue phase III: Topological fluid of skyrmions, *Phys. Rev. X* **12**, 011003 (2022).  
 [12] P. Sheng, Phase transition in surface-aligned nematic films, *Phys. Rev. Lett.* **37**, 1059 (1976).  
 [13] H. Yokoyama, Nematic–isotropic transition in bounded thin films, *J. Chem. Soc., Faraday Trans. 2* **84**, 1023 (1988).  
 [14] S. Kralj, A. Zidanšek, G. Lahajnar, S. Žumer, and R. Blinc, Phase behavior of liquid crystals confined to controlled porous glass studied by deuteron NMR, *Phys. Rev. E* **57**, 3021 (1998).  
 [15] K. Kočevar, A. Borštnik, I. Mušević, and S. Žumer, Capillary condensation of a nematic liquid crystal observed by force spectroscopy, *Phys. Rev. Lett.* **86**, 5914 (2001).  
 [16] U. Singh, P. J. Collings, C. J. Booth, and J. W. Goodby, Static and dynamic light scattering near the liquid crystalline blue phase III—nematic liquid critical point, *J. Phys. II (France)* **7**, 1683 (1997).  
 [17] J. Fukuda, A. Nych, U. Ognysta, S. Žumer, and I. Mušević, Liquid crystalline half-skyrmions and their optical properties, *Ann. Phys. (Berlin)* **534**, 2100336 (2022).  
 [18] See Supplemental Material at <http://link.aps.org/supplemental/10.1103/PhysRevLett.132.178101> for experimental details and further discussion, which includes Refs. [11,14,19–33].  
 [19] M. Arko and A. Petelin, Cross-differential dynamic microscopy, *Soft Matter* **15**, 2791 (2019).  
 [20] A. Poniewierski and T. J. Sluckin, Theory of the nematic-isotropic transition in a restricted geometry, *Liq. Cryst.* **2**, 281 (1987).  
 [21] V. Popa-Nita and T. J. Sluckin, Kinetics of the nematic-isotropic interface, *J. Phys. II (France)* **6**, 873 (1996).  
 [22] I. M. Syed, G. Carbone, C. Rosenblatt, and B. Wen, Planar degenerate substrate for micro- and nanopatterned nematic liquid-crystal cells, *J. Appl. Phys.* **98**, 034303 (2005).  
 [23] F. Nemoto, I. Nishiyama, Y. Takanishi, and J. Yamamoto, Anchoring and alignment in a liquid crystal cell: Self-alignment of homogeneous nematic, *Soft Matter* **8**, 11526 (2012).  
 [24] F. Giavazzi, D. Brogioli, V. Trappe, T. Bellini, and R. Cerbino, Scattering information obtained by optical microscopy: Differential dynamic microscopy and beyond, *Phys. Rev. E* **80**, 031403 (2009).  
 [25] F. Giavazzi and R. Cerbino, Digital fourier microscopy for soft matter dynamics, *J. Opt.* **16**, 083001 (2014).  
 [26] F. Giavazzi, S. Crotti, A. Speciale, F. Serra, G. Zanchetta, V. Trappe, M. Buscaglia, T. Bellini, and R. Cerbino, Viscoelasticity of nematic liquid crystals at a glance, *Soft Matter* **10**, 3938 (2014).  
 [27] G. Poy, Hidden traces of chirality in the fluctuations of a fully unwound cholesteric, *Soft Matter* **19**, 1115 (2023).  
 [28] A. Petelin, Cross-differential dynamic microscopy, v. 0.1.2 (2020), [10.5281/zenodo.3755036](https://doi.org/10.5281/zenodo.3755036).

- [29] A. K. Sen and D. E. Sullivan, Landau de Gennes theory of wetting and orientational transitions at a nematic-liquid substrate interface, *Phys. Rev. A* **35**, 1391 (1987).
- [30] P. Oswald and G. Poy, Droplet relaxation in Hele-Shaw geometry: Application to the measurement of the nematic-isotropic surface tension, *Phys. Rev. E* **92**, 062512 (2015).
- [31] S. Faetti and V. Palleschi, Measurements of the interfacial tension between nematic and isotropic phase of some cyanobiphenyls, *J. Chem. Phys.* **81**, 6254 (1984).
- [32] P. G. de Gennes and J. Prost, *Physics of Liquid Crystals* (Oxford University Press, New York, 1995).
- [33] I. Muševič, *Liquid Crystal Colloids* (Springer International Publishing AG, New York, 2017).
- [34] J. Pišljarić, M. Marinčič, S. Ghosh, S. Turlapati, R. Nandiraju, A. Nych, M. Škarabot, A. Mertelj, A. Petelin, A. Pusovnik, M. Ravnik, and I. Muševič, Skyrmions in blue phases of chiral liquid crystals, *Liq. Cryst.* **50**, 1406 (2023).
- [35] R. Cerbino and V. Trappe, Differential dynamic microscopy: Probing wave vector dependent dynamics with a microscope, *Phys. Rev. Lett.* **100**, 188102 (2008).
- [36] *Soft Matter Physics*, edited by M. Kleman and O. D. Lavrentovich (Springer, New York, 2004).
- [37] W. Cochran, *Structural Phase Transitions and Soft Modes*, edited by E. J. Samuelsen, E. Andersen, and J. Feder (Scandinavian University Books, Oslo, 1971).
- [38] A. Borštnik Bračič, K. Kočevar, I. Muševič, and S. Žumer, Capillary forces in a confined isotropic-nematic liquid crystal, *Phys. Rev. E* **68**, 011708 (2003).
- [39] H. Stark, J. Ichi Fukuda, and H. Yokoyama, Capillary condensation in liquid-crystal colloids, *Phys. Rev. Lett.* **92**, 205502 (2004).
- [40] P. Oswald and P. Pieranski, *Nematic and Cholesteric Liquid Crystals* (CRC Press, Boca Raton, 2005).
- [41] K. Kočevar and I. Muševič, Forces in the isotropic phase of a confined nematic liquid crystal 5CB, *Phys. Rev. E* **64**, 051711 (2001).
- [42] M. Nespoulous, C. Blanc, and M. Nobili, Orientational quenched disorder of a nematic liquid crystal, *Phys. Rev. Lett.* **104**, 097801 (2010).
- [43] C. Long and J. V. Selinger, Explicit demonstration of geometric frustration in chiral liquid crystals, *Soft Matter* **19**, 519 (2023).
- [44] W. Zurek, Cosmological experiments in condensed matter systems, *Phys. Rep.* **276**, 177 (1996).